

EVALUATION OF PHYSICAL AND MECHANICAL PROPERTIES AT CELL WALL LEVEL WITH NEW MICROSCOPY TOOLS

Bruno Clair & Bernard Thibaut

LMGC – Bois, CNRS / Université Montpellier II
CC 048, Place E. Bataillon, 34095 Montpellier, France.
(e-mail: thibaut@lmgc.univ-montp2.fr)

SUMMARY

In order to evaluate differential strains between wood cell wall layers, both stereo scanning electronic microscopy images and atomic force microscopy topographic images were used. G layer in tension wood shows a more important longitudinal shrinkage than other layers. Environmental scanning electron microscopy proved useful to analyse the different shrinkage kinetics between G layer and the other wall layers.

Atomic force microscopy in modulation mode is a powerful tool to estimate the relative rigidity of the different cell wall layers with a very high resolution. But, more theoretical work should be done in order to have absolute values of these MOE by comparison to isotropic standards. For wet wood, acoustic microscopy in transmission mode, at frequencies around 1 GHz, can be used for absolute measurements of MOE with a resolution of 1 μm . A new transmission acoustic microscope design is presented.

Key words: Wood properties, SEM, ESEM, Acoustic microscopy, Atomic Force Microscopy, cell wall

INTRODUCTION

When looking at wood behaviour in changing environment (ie temperature and moisture content changes) in the longitudinal direction, there is strong evidence that most of the phenomena explaining longitudinal strains and specific modulus of elasticity (MOE divided by density) come from the cell wall itself.

Models have been built to try and explain cell properties from cell wall layers' behaviour (Yamamoto 1999, Gril et al 1999, Harrington et al 1998). In order to compare these models to reality and to get realistic values of each layer's parameters, there is a need for experiments at the cell wall level.

Scanning electron microscopy (SEM or ESEM), scanning acoustic microscopy (SAM) and atomic force microscopy (AFM) can be used either for differential strain or for rigidity measurements.

I - DIFFERENTIAL STRAINS BETWEEN WALL LAYERS

Cell wall layers have distinctive architecture of main components (nano fibres and matrix) and chemical composition. Maturation strain can be different in each layer (thus leading to residual stresses at the very cell wall level).

Moreover, every change in temperature and moisture content (hygrothermal recovery in wet state or hygroscopic shrinkage during drying) induces hygrothermal strains which can be different in each layer. These local phenomena give rise to macroscopic strains that can be measured with classical transducers or callipers.

Although longitudinal hygroscopic shrinkage is usually low (0.2%) it can change significantly between species and, within a tree, mostly between juvenile and mature wood or normal and reaction wood.

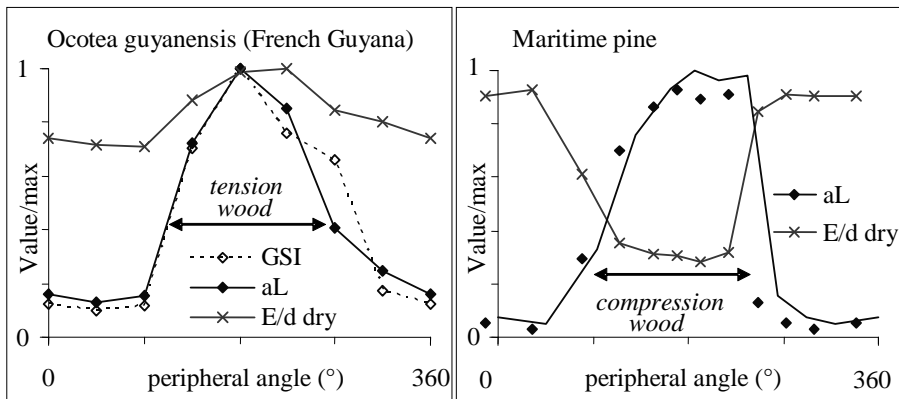


Fig. 1 : Longitudinal shrinkage and specific MOE for normal and reaction wood. Wood specimens come from different angular position at trunk periphery of the same tree evidencing a clear sector of reaction wood after measuring growth stresses in situ. Right: softwood with compression wood, left hardwood with tension wood. On the Y axis, values of the parameters are divided by the maximum one. GSI: growth stress indicator; aL: longitudinal shrinkage; E/d dry: specific MOE at 12% moisture content for wood.

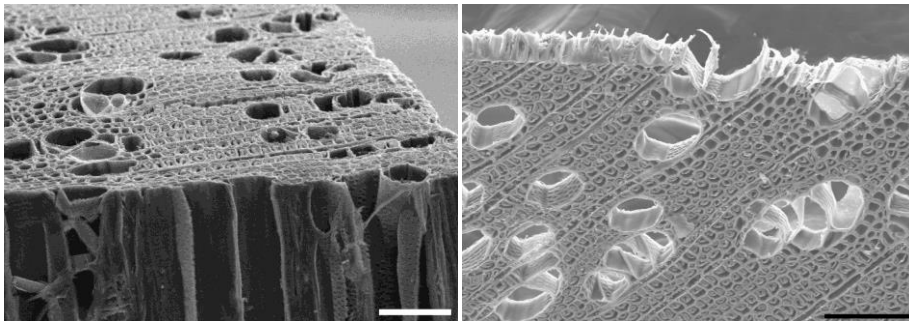
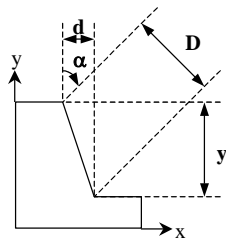


Fig. 2: SEM images of poplar: A solid bloc, B thin section; scale bars: 100 µm.

Classical models (Cave 1972, 1978) explain these changes from microfibril angle variations in S2 layer, which also explain the decrease in specific MOE. However, they cannot be used to explain the high longitudinal shrinkage in tension wood where specific modulus is higher than in normal wood (fig.1).

This problem was investigated on tension woods exhibiting classical G layer fibres: poplar (*Populus* cv I4551) and beech (*Fagus sylvatica* L.).



Equation 1:

$$y = \frac{D}{\sin \alpha} - \frac{d}{\tan \alpha}$$

d is the measured distance on normal image, D on the tilted 70° image and $\alpha = 70^\circ$

Fig. 3: Principle for calculation of topographic profiles

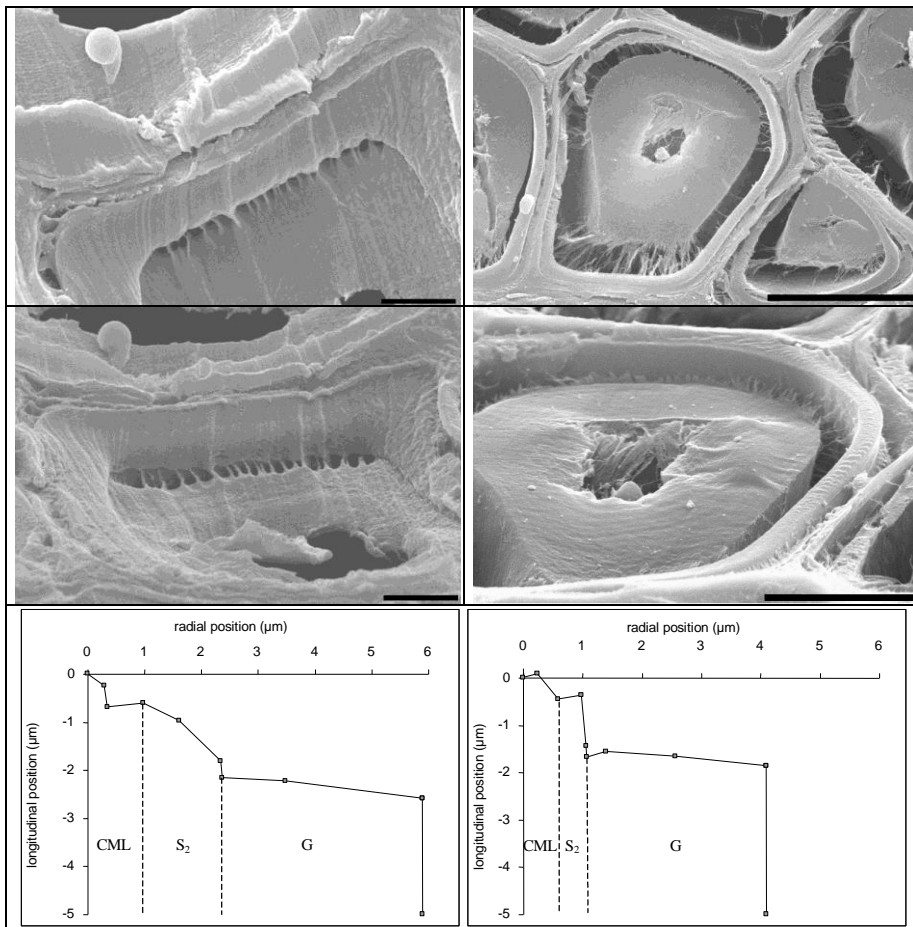


Fig. 4: SEM images and topographic profiles for one cell of beech (A, C, E) and poplar (B, D, F). A & B: normal to surface images; C & D: 70° oblique images. Scale bars: A & C: 2 μm , B: 10 μm , D: 5 μm . (CML: compound middle lamella).

Stereo scanning electron microscopy

Solid blocks (5 mm size cubes, fig.2 A) and thick sections (80 μm thick) are cut and glued in wet condition (in water). Sections are glued on their edge with the fibre

direction parallel to the support, in order to allow observations on transverse sections on both sides of the sample (fig 2 B). Samples were dehydrated with absolute ethanol, passed to critical point and coated (300 Å of platinum) before observation. Thus, observations were made in oven dry condition with a Cambridge S360 Scan Electron Microscope.

Tilting the receptor allows images of a same object obtained for different view angles. Both in poplar and beech, one cell is observed with two angle of view, at first perpendicular to the surface and then tilted 70° from that direction (Fig. 4). From these two images of the same cell, it is possible to draw a topographic profile of the cell after shrinkage. The x coordinate is given directly by the first image while the y coordinate can be calculated with equation 1 using both images (Fig. 3).

These topographic profiles allow measurements of differential shrinkage between cell wall layers. Notably, G layers are far more retracted than other layers (mean 2.2 µm in beech and 2.8 µm in poplar).

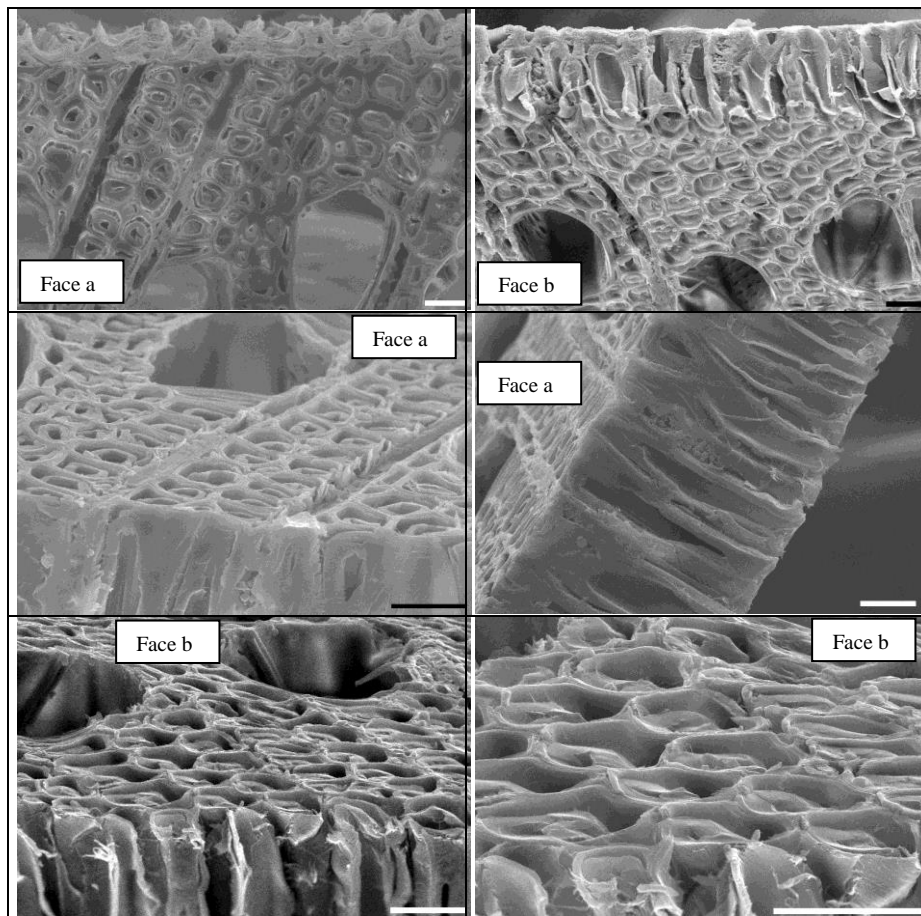


Fig. 5: SEM images of both faces of poplar section with different scales and view angles. Some cells on the edge (arrow) allow to locate all others. A & C: face a, B, E & F: face b. Measurements are made on images like F (Scale bars: 20 µm).

In the S_2 layer of beech there seem to be a strain gradient from the S_1 to the G layers, which is not the case for poplar (fig. 4).

In the thick sections several poplar cells were observed after drying. Restraint measurements have been made in the same cells on both faces of the section. To this aim, numerous images have been taken with different scales and view angles to locate the cells (fig. 5). Mean measurements of differential restraint between G layer and compound middle lamella (CML) are $1.99\text{ }\mu\text{m}$ for a face, $1.83\text{ }\mu\text{m}$ for the other and $3.82\text{ }\mu\text{m}$ for the sum of faces. Thus, the total G layer differential shrinkage can be estimated between 3.6 % and 5.8 % with a mean value of 4.7 % , using the ratio between summation of both retrains and section thickness ($80\text{ }\mu\text{m}$).

Atomic force microscopy

Smaller solid blocks ($500 \times 500 \times 500\text{ }\mu\text{m}^3$), prepared the same way as before, have been observed in their transverse section in water and in air-dry condition.

Four states have been studied: green condition, green condition after 2 hours in 80°C water, air-dry conditions, wet conditions after air-drying. The Atomic Force Microscope (Dimension 3100, Nanoscope IIIa, Digital Instruments) was used to obtain topographic images of a $50 \times 50\text{ }\mu\text{m}^2$ area (around 10 cells). The same cells have been observed successively in these conditions (Fig. 6).

The profile in water (Fig. 6 A') shows that there is already a small retraction of the G layer before drying. This can be due to the release of residual stresses between layers after cross cutting but also to cutting artefacts linked to differences in hardness between the layers.

The profile in water after 2 hours in 80°C water (Fig. 6 B') shows very little additional retraction of the G layer before drying. This could be related to a very small longitudinal HTR (Kübler 1987, Gril & Thibaut 1994).

The profile in air-dry conditions (Fig. 6 C') confirms the presence of a more important shrinkage in the G layer than in other layers. It can be noted also that, after drying, shrinkage is more important in the middle lamella than in the S_2 layer.

The profile in wet conditions after air-drying (Fig. 6 D') shows a swelling of the G layer which allows it to almost recover its green condition position. Another profile (not shown), in air-dry conditions again, shows the reversibility of the phenomenon.

Environmental scanning electron microscopy

In order to have a look at shrinkage kinetics, observations were made with the same material (poplar cubes 1mm size) in ESEM, beginning with the wet specimen not glued on the support in order to have free transverse shrinkage during the change in temperature and vacuum pressure in the chamber (from 4°C to 25°C and 5 Torr to 2 Torr).

Two phases were observed. In the first one (20 to 30 minutes) water firstly goes out of the lumen and there is a strong contraction of the G layer in all transverse directions. This G layer remains in close contact to the other layers and, globally, there is very little overall shrinkage (around 1%) of the whole tissue (fig. 7). In the second one, beginning with the partial separation of G layer from the other layers, the global geometry of the cells changes and there is a significant tangential shrinkage (around 5%) while there seems to be no more G layer thickness changes (fig. 8).

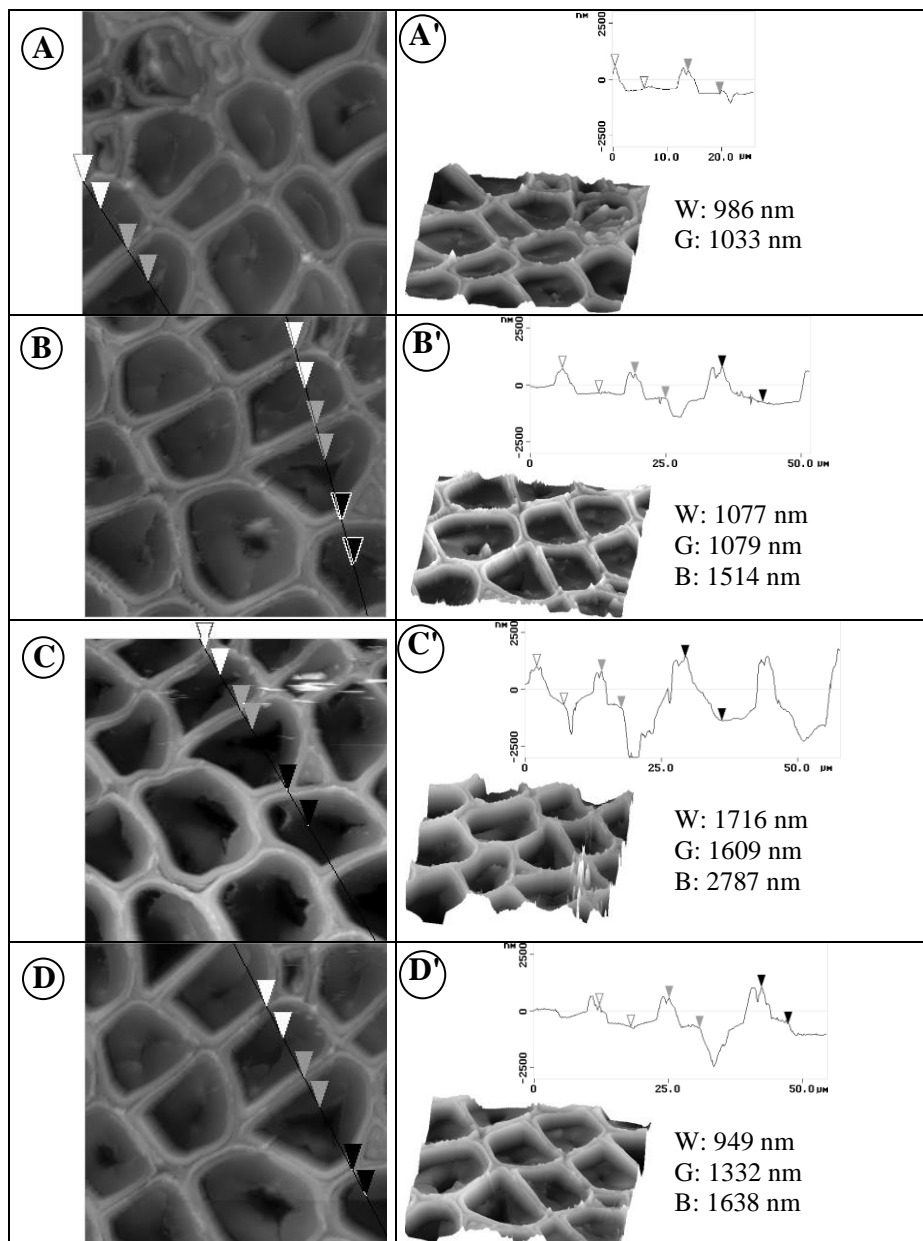


Fig. 6: measurements on AFM topographic profiles of same poplar cells in water (A), in water after 2 hours in 80°C hot water (B), in air dry condition (C) and in water after drying (D). Vertical distance between S_2 layer and G-layer: W: white cursors, G: grey cursors, B: black cursors.

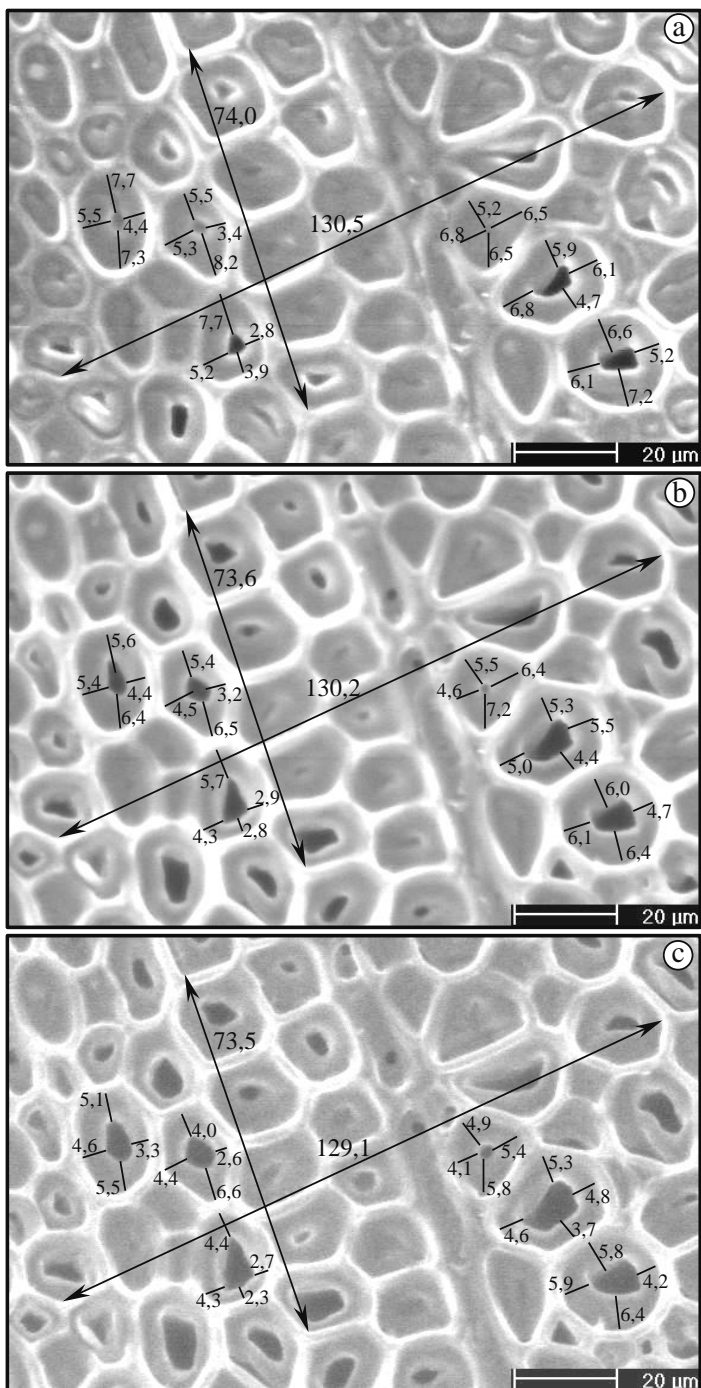


Fig. 7 : shrinkage of G layer during first phase of drying in ESEM ; a is just after the departure of the thin film of water covering the specimen ; b & c are two successive drying steps at 10 minutes interval. Thickness measurements are in μm.

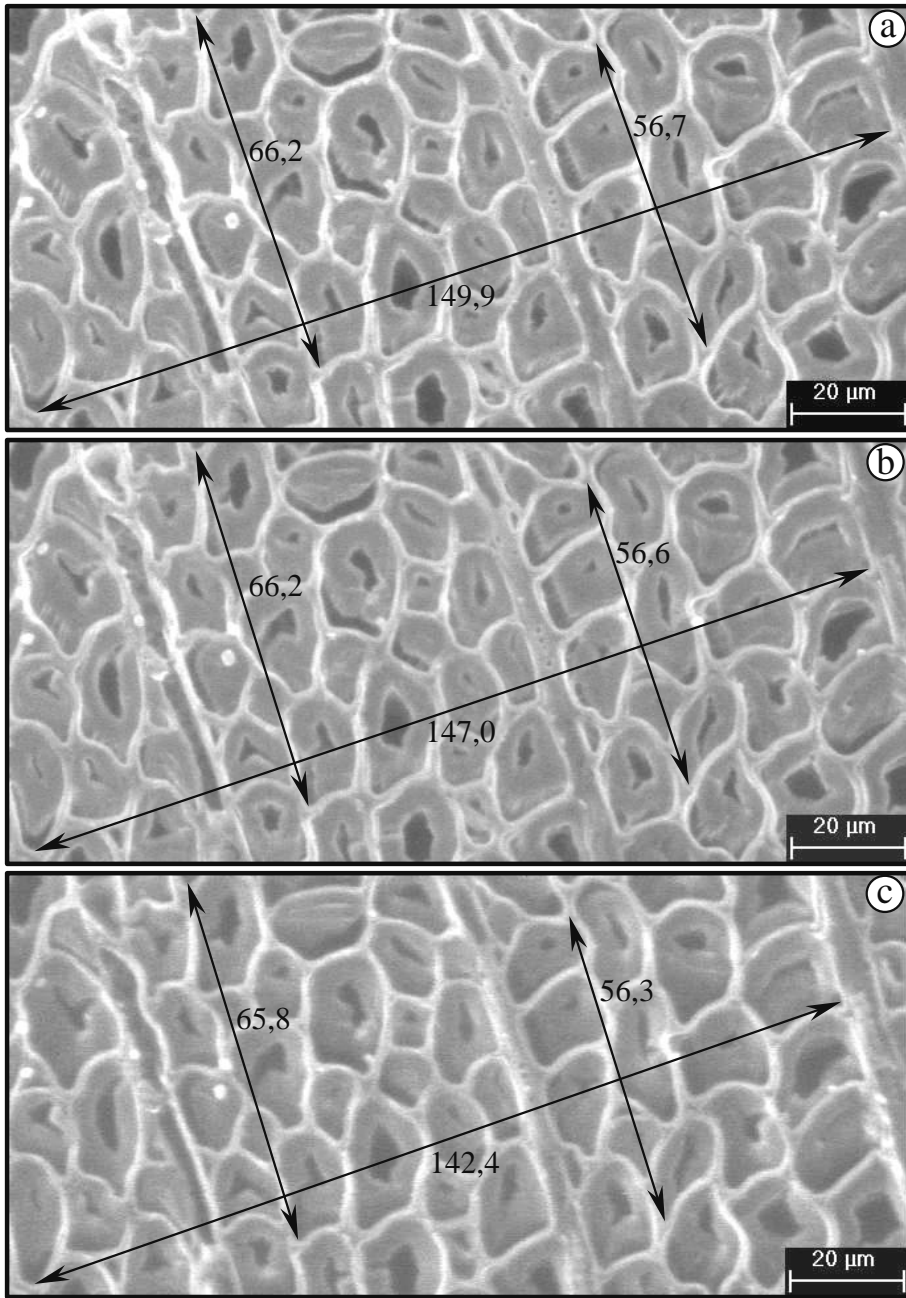


Fig. 8 : shrinkage in the second phase in ESEM on the same group of cells; measurements in μm.

II – RIGIDITY OF CELL WALL LAYERS

Atomic force modulation microscopy

Local measurements by nanoindentation reported by Wimmer & Lucas (1997) and Wimmer et al. (1997), show the fact that mechanical properties of each cell layer can be estimated, at least those with sufficient thickness to be considered as semi-infinite at the scale of the indenter.

This can be done also using the technique introduced by Yamanaka & Nakano (1996) and Rabe et al. (1996) and called Force Modulation Microscopy or Acoustic Force Microscopy.

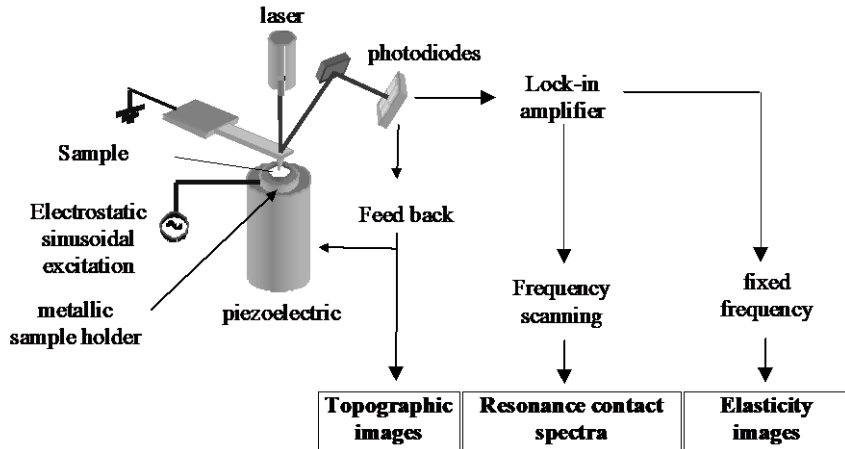


Fig.9. Schematic representation of an atomic force microscope in force modulation mode.

The device used is a commercial AFM (Digital Instruments Nanoscope 3100) whose tip is in contact with the sample (Fig.9). The lever geometry is described by its length ($L=130\text{ }\mu\text{m}$), its width ($W=35\text{ }\mu\text{m}$) and its thickness ($h=1\text{ }\mu\text{m}$); it has a low spring constant in bending ($k=0.67\text{ N/m}$) and a free oscillation frequency of 65 kHz. The tip length is about 15 μm and the radius at the apex is of the order of $R=30\text{ nm}$ for a new tip, which increases by wear up to $R=600\text{ nm}$. Lever and tip are in crystalline silicon, coated with a thin WC layer in order to minimise its wear.

The contact force between the tip and the sample is detected with a laser beam that reflects on the lever and is received by photodiodes. During the scan on the sample, the feedback of the microscope maintains a constant contact force. This allows acquisition of the topography of the surface, by recording the movements of the piezoelectric actuators during the scans.

Simultaneously, a periodic force is applied on the lever, by means of an electrostatic potential applied to the sample holder. When the excitation frequency is close to the proper frequency of the lever a resonance occurs. The resonance frequency is related to the geometry and the stiffness of the contact, which can then be deduced.

The lever oscillation frequency (in the 500 kHz to 1 MHz range) being much higher than the force feedback response time, the topographic information can be separated from local variations of the mechanical property. Hence, then the sample stiffness and topography can be collected simultaneously.

The equations governing the oscillation of the cantilever and the tip are thoroughly analysed by Rabe et al. (1998), Yamanaka & Nakano (1998), Pietrement & Troyon

(2000b) and Dupas et al. (2001). For each cantilever a master curve can be build, relating the resonance frequency to the contact impedance “s” on the sample. The Hertz or DMT contact theories (Maugis 2000; Pietrement & Troyon 2000a) allow then an evaluation of the reduced elastic modulus E of the sample, assuming an isotropic sample and a rigid tip :

$$s = \frac{dF}{d\delta} = \frac{d}{d\delta} \left(\frac{4}{3} E^* R^{1/2} \delta^{3/2} \right) = 2E^* R^{1/2} \delta^{1/2} = (6E^* 2RF)^{1/3}$$

R is the tip radius, δ the penetration, F the contact force, and E^* the reduced Young modulus (indentation modulus) $E^* = E / (1 - \nu^2)$. The tip is supposed to be perfectly rigid. Note that the contact force F includes the known applied force, the adhesion + capillary forces, and the mean electrostatic force used to excite the cantilever. The total force is estimated for each experiments (by pulling away the tip up to break the contact) and ranges between 10 and 100 nN, depending on the tip apex conditions.

Many sources of uncertainty arise in the experiments. First of all is the uncertainty of the cantilever characteristics as given by the manufacturers, dispersion of a factor 2 is common for the cantilever stiffness. Secondly, the exact shape of the tip apex may differ notably from a sphere (even for a new tip) and may evolve by wear during the scans towards a flatter surface. Obtaining an image with a constant radius is not so easy and regular tip change and subsequent re-calibration are needed.

In conclusion, calibration of the elastic properties of the sample cannot be done by using theoretical models only, but needs to be compared to standard samples of known properties. Several homogeneous samples, with properties encompassing the wood expected values were selected and measured (by acoustic methods) : gold ($E^* = 95$ GPa) , Pyrex glass ($E^* = 62$ GPa), sulphur ($E^* = 13$ GPa) , PMMA ($E^* = 6.5$ GPa) and Polyurethane ($E^* = 0.28$ GPa). The properties of the wood are obtained by interpolation, with a master curved fitted on the known samples.

Measurements have been carried out on holm oak (*Quercus ilex* L.) wood in a zone including fibres with gelatinous layer where both G and S2 layers are thick

A small sample is produced and glued perpendicularly to the fibres on the sample holder by cyanoacrylate glue (gel form). The four faces of the sample are then cut to give the shape of a cube $1 \times 1 \times 1$ mm³. A final surface finish is given to the upper face with a new disposable microtome blade.

The upper surface must be as flat as possible, because too much roughness would modify the contact surface between the tip and the sample and affect the elastic measurements.

The wood samples are cut in air dry conditions and measures are made after stabilization of the sample in ambient air.

An excitation frequency for which the amplitude variations generates good contrast is chosen and the sample is scanned at this frequency. A picture of "elastic contrast" is recorded, as the oscillation amplitude of the cantilever during the topographic scans.

A scan in frequency performed at some fixed point on the sample is then used to measure precisely the resonance frequencies there.

Measurement of the resonance frequency on the standard samples should be done just before and just after, to have a good calibration.

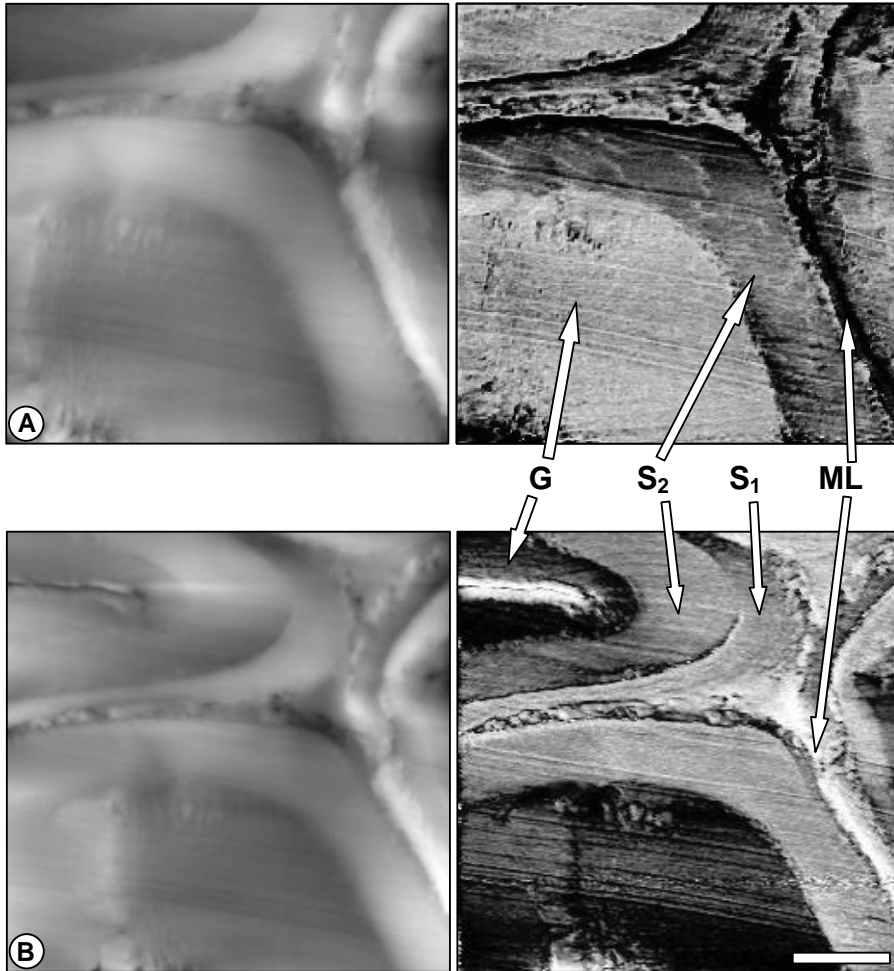


Fig 10. Cell wall layers of oak tension wood. In topographic images (on the left), grey levels span a total of 300 nm. The "elasticity" images (on the right) were taken at 620 kHz (A) and 690 kHz (B). At 620 kHz, the lighter zone corresponds to the stiffer cell wall layers, while the reverse occurs at 690 kHz (B). Scale bar = 2 μ m.

For valid results, the applied force and tip shape must not have changed during the three steps, the last condition appearing to be the most difficult to achieve. Examples of curves of the amplitude versus frequency are presented in Fig 11, for a typical cell (4 points on G layer, 4 on S₂, 2 on S₁ and 2 on middle lamella).

A small dispersion of the resonance frequencies within each cell wall layer and a drift toward higher values of frequency from the external layers toward the internal ones (ML toward G) can be noticed. This gives a qualitative information on stiffness: G layer being the most rigid and middle lamella ML the least. These qualitative results are in agreement with the classic description of these layers (microfibril angle and crystalline cellulose content).

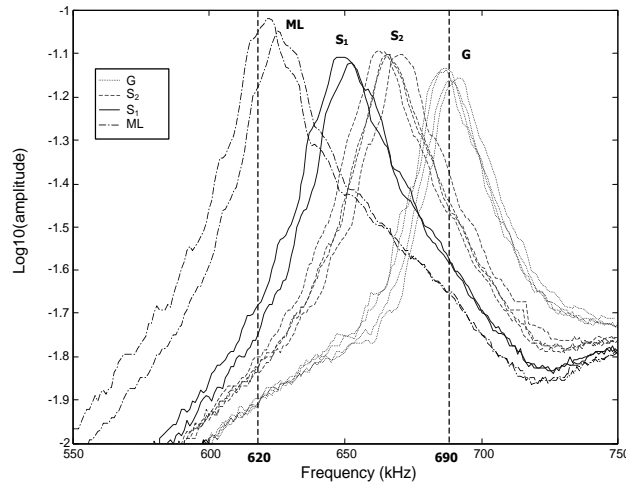


Fig. 11. Resonance spectra on the different cell wall layers of holm oak fibre.

The two pictures presented in Fig 10 are obtained at two different fixed frequencies for and show how the contrast depends on the working frequency. At 620 kHz, the amplitude of the tip is maximum on the soft middle lamella, and low on the stiff G layer. At 690 kHz the reverse contrast occurs.

The pictures show a large contrast between the wood cell wall layers, each layer being characterised by a relatively constant stiffness. The lateral resolution of the elastic images is of the order of 20 to 50 nm and is determined by the radius of the contact area between the tip and sample.

Quantitative results obtained by comparison with standard samples, as explained above, are reported in Table 1, together with results obtained by Wimmer and Lucas (1997) and optimal values used by Harrington et al. (1998) or Watanabe and Norimoto (2000) to get realistic values of wood elastic modulus from models based on micro/macro approach.

The results are rather similar to those obtained by nanoindentation. Wimmer et al. (1997) found large variations of elastic modulus in each cell wall layer for the different measurements (1 to 3 in proportion). Such variations (1 to 2) were also found between different measurements on the same species (holm oak). But, for a same set of measures or for one or two adjacent cells, variations are limited to a maximum of 20 % in each cell wall.

It should be noted that: i) relative values between ML, S_1 and S_2 are similar in nearly all the cases; ii) longitudinal elastic modulus estimated, both by indentation and atomic force microscopy in force modulation mode are significantly lower than values used in good models (up to five times less).

On one hand, a partial explanation can come from the actual values of MFA for the specimens used in the experimental work (spruce in one case, holm oak in the other), but normally the G layer should have a high MFA.

On the other hand, the elastic moduli in both cases (AFM) were calculated with the assumption of elastic isotropic behaviour of the cell walls, which is surely not the case. Oliver and Pharr (1992), discussing about the use of nanoindentation for different materials, pointed out some discrepancy between elastic modulus measured by this method and reference values, for anisotropic materials (sapphire and quartz). They argued that in this case, using isotropic simplification can lead to values intermediate between elastic modulus in the two direction of anisotropy.

Table 1 Measured elastic properties of the cell layers, in GPa , expressed as the indentation modulus $E^*=E / (1-\nu^2)$ or as the Young modulus E for extension experiments. (r = radius of curvature of tip, *our experimental results corresponding to the presented curves and images, **other experimental results, *** measured on cell corner).

		ML	S1	S2	G
holm oak wood fibre*	r = 30 nm	5 - 7	8 - 9	9 - 10	10 -12
other holm oak wood fibre**	r = 40 nm	15		20	
other holm oak wood fibre**	r = 600 nm	7 - 8		9 - 10	
boco wood fibre**	r = 400 nm	10		12 - 18	
Wimmer & Lucas (1997) on spruce wood	pyramid indentation	5-15***		7 - 22	
Harrington (1998)	model and assumptions	18	53	64 (MFA=0°)	
Watanabe (2000)	simulation	33	54	64 (MFA=0°) 10 (MFA=40°)	

In the case of highly anisotropic fibre reinforced polymers like cell walls, a 10 to 20 ratio between elastic modulus in transverse and longitudinal direction is often found. So calculated values of elastic modulus using isotropic elastic contact (which is the case in both methods) can lead to values lying somewhere between one and one tenth of the longitudinal expecting one.

Basic mechanical analysis is needed to fully understand what is really measured with these techniques for cell wall material. Measurements on both transverse cell section, like in this study, and longitudinal (radial or tangential) cell section will be necessary to estimate the elastic modulus in the two main direction of anisotropy in the cell walls at the same time.

However, AFM techniques have a high potential in the future to investigate mechanical properties at the cell wall levels for absolute values or for comparisons between walls or between cells representative of different types (juvenile/mature ; spring/summer or normal/reaction wood).

The two methods discussed here seem complementary. Nanoindentation uses very hard (diamond) tips with well known geometry and rather stable. It has a higher potential to obtain quickly a good absolute estimate of local elastic properties on a given set of positions. Atomic force microscopy in force modulation mode uses softer (silica) tips which will be more or less quickly blunted during operation. Probably using blunted tips with 100 to 500 nm radius will be a better solution to limit variations in image acquisition. It has a higher ability to perform high resolution images of elastic constant for cell walls with a reliable relative estimation of elasticity between regions.

Furthermore, it should be possible to have an idea of the damping properties of each cell wall layer by using time X frequency analysis and relevant viscoelastic models for anisotropic materials.

Transmission acoustic microscopy

Transmission or reflection of acoustic waves in different materials are ways to estimate viscoelastic properties by measuring sound velocity or damping. To obtain high resolution images, very high frequencies are needed (1 GHz for 1 μm resolution). At these frequencies, damping of soft biological material like wood becomes too high for the use of reflection microscopy, which has been developed for metals or ceramics (Saurel et al. 1989, Bereither-Hahn 1995, Clair et al. 2000). A new transmission acoustic microscope was designed and built for this purpose. Principle of transmission acoustic microscope is shown on figure 12.

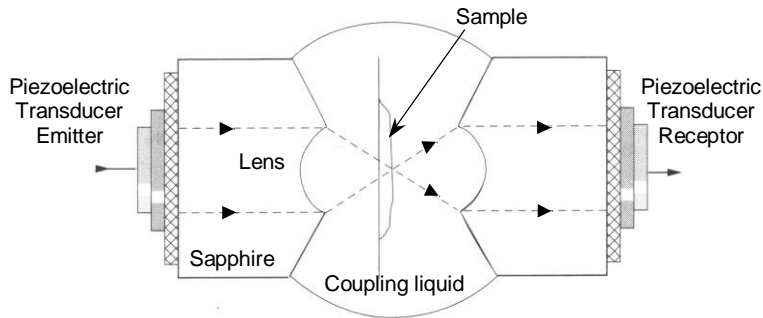


Fig. 12: Acoustic wave path between the two transducers in transmission mode.

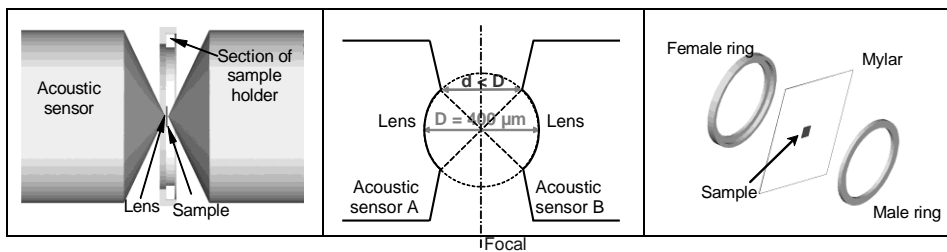


Fig. 13: Position of the specimen between acoustic transducers.

The wood specimen is a thin slice (12 μm) glued on a mylar sheet with a 1mm diameter hole in the middle (sound path). This mylar sheet is held on a specific device attached to the vibrating cell (fig. 13). The specimen should be placed right in the middle between the two symmetric acoustic transducers.

This positioning and the alignment of the two transducers should be done with very high precision (0.5 μm), so the kinetic chain in the 3 directions is critical. Piezoelectric moving devices are used to obtain these very precise positioning (and repositioning after the choice of the observed zone).

Furthermore, a small optical microscope with a CCD camera is added to visualise the specimen before acoustic imaging, in order to choose the cells to be measured (fig. 14).

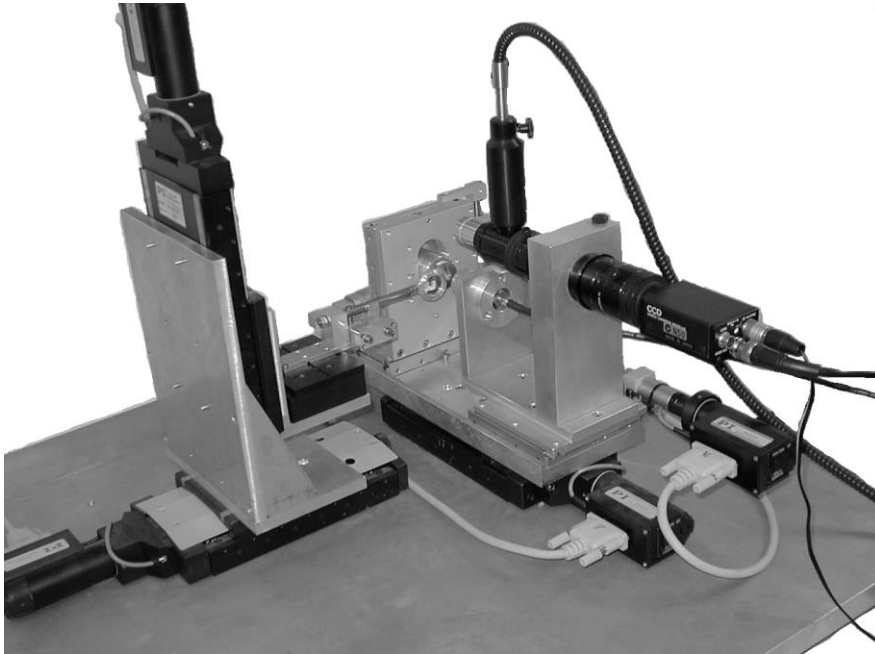


Fig. 14: Photo of the new scan transmission acoustic microscope

For the electronic part of the system, some innovation was also necessary in order to get a very precise definition of frequency (around 1 GHz) and sound velocity (fig.15).

The connecting device allows to work both in transmission and in reflection mode. The synchro system is used to coordinate acoustic burst emissions and motorised displacements of the sample. The signal processing, at the end of the operation gives different data such as specimen thickness, sound velocity and damping on every dot of the image.

To estimate specimen thickness, flying time of the sound burst is measured both in reflection and transmission. A validation of those methods was performed on a copper electronic grid (250 X 200 μm) whose thickness was 13.2 μm .

The first tests were done on beech wood with acoustic transducers usually dedicated to reflection microscopy (fig. 16). Three kind of images are provided: attenuation patterns (fig. 16-a); grey levels are inversely proportional to sound damping in cell wall (compound middle lamella is damping more than S2 layer); flying time through specimen (fig. 16-b); grey levels are inversely proportional to sound velocity, which is directly linked to the square root of the ratio MOE / Density; phase images (fig. 16-c) provide another way of measuring sound velocity, with a somewhat higher precision useful for thickness measurement.

The image quality is rather poor compared to what should be expected with this device. This is due to the use of acoustic transducers not fully dedicated to transmission microscopy. On the one hand these transducers should be very finely matched one to the other for symmetry reasons, and this was not the case for the two transducers used in reflection mode where each one works alone. On the other hand, low open angle acoustic transducers should be manufactured for this application. This is in progress.

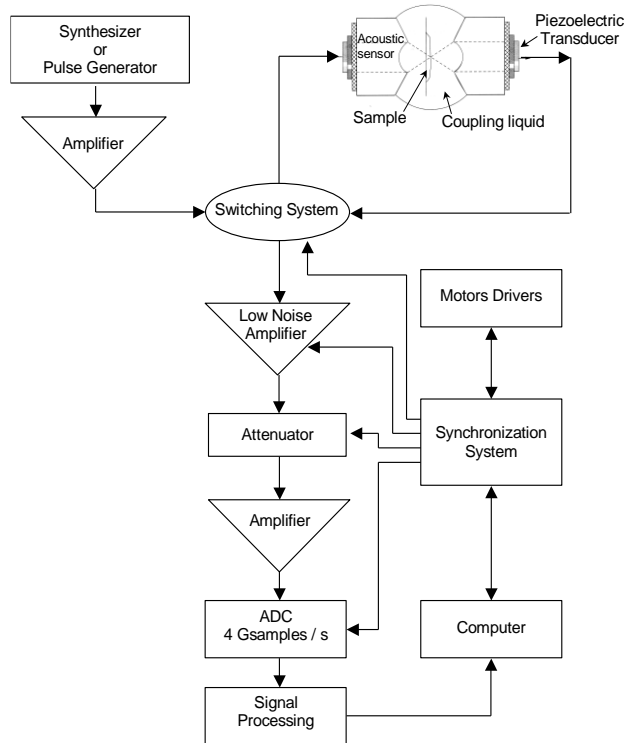


Fig. 15: Synoptic diagram of the transmission acoustic microscope

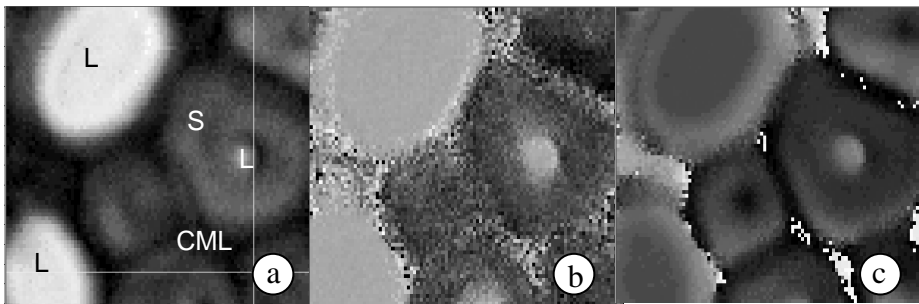


Fig. 16: Transmission acoustic images of beech wood cells ($30 \times 30 \mu\text{m}^2$). a: attenuation image; b: time of flight image; c: time of flight image using the phase ($\pm 2\pi$) L: lumen, S: secondary wall, CML: Compound middle lamella

Compared to AFM measurements, acoustic microscopy can be easily performed in wet state (using water as coupling agent between the two lenses), or in other liquids known to modify wood (or cell wall layers) behaviour. Furthermore, as was stated before, all these experimental methods are indirect measurements of physical mechanical properties. Some models are always needed in order to get properties by inverse methods. Complementarities between experimental techniques appears then as a useful tool to gain confidence and assess “true” values for different layers, under different environmental conditions.

REFERENCES

- Bereiter-Hahn, J. 1995. Probing Biological Cell and Tissues with Acoustic Microscopy. *Advanced in Acoustic Microscopy*. A. Briggs. New York and London, Plenum Press. 1: 79 -110.
- Cave, I.D. 1972. A Theory of the Shrinkage of Wood. *Wood Science and Technology*, 6: 284-292.
- Cave, I.D. 1978. Modelling Moisture-Related Mechanical Properties of Wood. Part I: Properties of the Wood Constituents. *Wood Science and Technology*, 12: 75-86.
- Clair, B., G. Despaux, B. Chanson & B. Thibaut. 2000. Utilisation de la microscopie acoustique pour l'étude des propriétés locales du bois : étude préliminaire de paramètres expérimentaux. *Annals of Forest Science* 57: 335-343.
- Clair, B. & B. Thibaut. 2001. Shrinkage of the gelatinous layer of poplar and beech tension wood. *IAWA Journal*, Vol. 22(2), 121-131.
- Clair, B., R. Arinero, G. Lévêque, M. Ramonda & B. Thibaut. (to be published). Imaging the mechanical properties of wood cell layers by atomic force Modulation microscopy. *IAWA Journal*.
- Dupas, E., G. Gremaud, A. Kulik & J.L. Loubet. 2001. High-frequency mechanical spectroscopy with an atomic force microscope. *Rev. Sci. Instrum.*, 72: 3891-3897.
- Gril, J., F. Sassus, H. Yamamoto & D. Guitard. 1999. Maturation and drying strain of wood in longitudinal direction: a single-fibre mechanical model. In: G. Nepveu (Editor), 3rd Workshop on Connection between silviculture and wood quality through modelling approaches and simulation softwares (IUFRO WP S5.01.04 "Biological Improvement of Wood Properties"). ERQB-INRA Nancy, La Londe-Les-Maures, pp. 309-313.
- Gril, J. & B. Thibaut. 1994. Tree mechanics and wood mechanics: relating hygrothermal recovery of green wood to the maturation process. *Annales des Sciences Forestières*, 51: 329-338.
- Harrington, J.J., R. Booker & R.J. Astley. 1998. Modelling the elastic properties of softwood (Part I : The cell-wall lamellae). *Holz als Roh- und Werkstoff*, 56: 37 - 41.
- Kübler, H. 1987. Growth stresses in trees and related wood properties. *Forest Products Abstracts*, 10: 61-119.
- Maugis, D. 2000. *Contact Adhesion and Rupture of Elastic Solids*. Springer, Berlin.
- Oliver, W.C. & G.M. Pharr. 1992. An improved technique for determining hardness and elastic modulus using load and displacement sensing indentation experiments. *J. Mater. Res.*, 7: 1564-1583.
- Pietrement, O. & M. Troyon. 2000a. General equations describing elastic indentation depth and contact stiffness versus load. *Journal of Colloid and Interface Science*, 226: 166-171.
- Pietrement, O. & M. Troyon. 2000b. Quantitative elastic modulus measurements by magnetic force modulation microscopy. *Tribology letters*, 9: 77-87.
- Rabe, U., K. Janser & W. Arnold. 1996. Vibration of free and surface coupled atomic force microscope: theory and experiments. *Rev. Sci. Instrum.*, 67: 3281-3293.
- Rabe, U., J. Turner & W. Arnold. 1998. Analysis of the high-frequency response of atomic force microscope cantilever. *Applied Physic*, A66: S277-282.
- Saurel, J. M., K. Alami, C. Amaudric du Chaffaut, O. Dugne & A. Guette. 1989. Mechanical characterisation by Acoustic Techniques of SiC CVD Thin Films. Conference of European Material Research Society, Strasbourg (France).

- Watanabe, U. & M. Norimoto. 2000. Three Dimensional Analysis of Elastic Constants of the Wood Cell Wall. *Wood Research*, 87: 1-7.
- Wimmer, R. & B.N. Lucas. 1997. Comparing mechanical properties of secondary wall and cell corner middle lamella in spruce wood. *IAWA bulletin*, 18: 77-88.
- Wimmer, R., B.N. Lucas, T. Tsui & O. W.C. 1997. Longitudinal hardness and Young's modulus of spruce tracheid secondary walls using nanoindentation technique. *Wood Science and Technology*, 31: 131-141.
- Yamanaka, K. & S. Nakano. 1996. Ultrasonic atomic force microscopy with overtone excitation of cantilever. *Jpn. J. Appl. Phys.*, 35: 3787-3792.
- Yamanaka, K. & S. Nakano. 1998. Quantitative elasticity evaluation by contact resonance in an atomic force microscope. *Applied Physic, A*: S313-S317.
- Yamamoto, H. 1999. A model of anisotropic swelling and shrinking process of wood. Part 1. Generalization of Barber's wood fiber model. *Wood Science and Technology*, 33: 311-325.